Applied Mathematical Modelling 39 (2015) 466–482

Contents lists available at ScienceDirect

Applied Mathematical Modelling

journal homepage: www.elsevier.com/locate/apm

Wave modes of a pre-stressed thick tube conveying blood on the viscoelastic foundation

Shueei-Muh Lin [a], Wen-Rong Wang [a,*], Sen-Yung Lee [b], Chien-Wi Chen [b], Yu-Cheng Hsiao [b], Min-Jun Teng [c]

[a] Mechanical Engineering Department, Kun Shan University, Tainan 710-03, Taiwan, ROC
[b] National Cheng Kung University, Tainan 701, Taiwan, ROC
[c] Mechanical Engineering Department, Guangzhou College of South China University of Technology, China

ARTICLE INFO

Article history:
Received 19 March 2011
Received in revised form 27 May 2014
Accepted 3 June 2014
Available online 16 June 2014

Keywords:
Artery
Dispersion curve
Energy propagation
Wave mode
Viscoelastic foundation

ABSTRACT

Wave propagation of an artery is a fluid–structure interaction problem. It is very complicate. Therefore, the conventional theories for circulation of arteries are emphasized on fluid behavior, some simplified models for experimental utility or the thin-walled tube theory. Based on the geometry of an artery, the thick-walled tube theory is reasonable. In this study, a new mathematical model is proposed to describe the wave propagation through the isotropic elastic thick tube filled with viscous and incompressible fluid. Moreover, the tube is supported by the elastic muscle and simulated as the viscoelastic foundation. The radial, axial and flexural vibrations of a tube wall are introduced simultaneously. These wave modes are generally called as the flexural, Young and Lamb modes. In the literatures according to different assumptions, the Young and Lamb modes were independently derived and independent to the wave frequency. Because these conventional models are over simplified, the corresponding investigations are incomplete and inaccurate. Moreover, the present thick-walled tube theory is compared with the thin-walled tube theory and these conventional limiting theories. The dispersion curves and the energy transmissions of the three modes are investigated. It is illustrate that the energy transmitted through the artery tube is consistent to the experiment. Moreover, it is found that the effects of the viscoelastic foundation constants on the wave speed and the transmission is significant. When the foundation constant is large enough, some corresponding mode will disappear.

1. Introduction

No matter animals or human beings, the blood circulation plays an important role in maintaining body working well. Many scientists investigated the heart vascular system, and proposed several theories and models to explain the performances of the blood circulation system. In general, the ratio of tube thickness to the tube radius of the artery of man or dog is from 0.06 to 0.13 [1]. The thick-walled tube theory should be considered for simulating the behavior of the artery. However, since the calculations appeared to be very laborious, the thin-walled tube theory was often introduced [2,3].

* Corresponding author. Tel.: +886 6 2050496; fax: +886 6 2050509.
E-mail address: me70ks10@mail.ksu.edu.tw (W.-R. Wang).

http://dx.doi.org/10.1016/j.apm.2014.06.002
0307-904X/

Nomenclature

A	surface area of the fluid element
c_{ij}	elastic constants
C_r, C_x	damping coefficients in the r- and x-directions, respectively
C_w	wave speed
D	diameter of the tube
E	Young's modulus
f	friction factor of the tube wall
G	shear modulus
h	thickness of the tube wall
k	wave number
K_r, K_x	elastic foundation constants in the r- and x-directions, respectively
L	tube length
M_{ij}	twisting moment perpendicular to i-plane along j-direction or perpendicular to j-plane along i-direction per unit length
M_x	bending moment perpendicular to x-plane along θ-direction per unit length
M_θ	bending moment perpendicular to θ-plane along x-direction per unit length
N_{ij}	shearing force perpendicular to i-plane along j-direction or perpendicular to j-plane along i-direction per unit length
N_x	normal force perpendicular to x-plane along θ-direction per unit length
N_θ	normal force perpendicular to θ-plane along x-direction per unit length
$\hat{n}$	normal direction of surface
p	liquid pressure at the wall
R	average radius of tube
Re	Reynold's number
R_i	inner radius of tube
R_o	outer radius of tube
r_{et}	percentage of energy propagations through the tube
t	time variable
u_r, u_θ, u_x	total displacements in r-direction, in θ-direction and in x-direction
u	displacement in x-direction
w	displacement in r-direction
$\vec{v}$	the flow velocity
V	volume of the fluid element

Greek symbols

β	angle due to bending
γ_{ij}	shearing strain on i–j plane
ε	normal strain
η	flow velocity distribution
υ	Poisson's ratio
ρ	density
σ	normal stress
τ_{ij}	shearing stress perpendicular to i-plane along j-direction
ω	wave frequency

Superscript, subscripts

–	amplitude
max	maximum quantity
r	radial coordinate
θ	transverse coordinate
x	axial coordinate
f	fluid
s	solid
0	static quantity due to pre-stressed
1	disturbed quantity due to wave propagation

Since Harvey [4] introduced the concept of the blood circulation, scientists have developed several vital theories. Hales [5] introduced the Winkessel model. The Winkessel model regards the whole arteries system as an elastic cavity. If the heart contracts, the cavity expands. In contrast, if the heart expends, the cavity recovers to original volume. It is expressed as the compliance–resistance model (C–R model). But the Windkessel model is only suitable for predicting pressure and volume of each contraction, and fails to evaluate flow velocity [6]. Assuming a steady and laminar flow and a rigid tube, the Poiseuille's equation explains the physical characteristics of the blood capillary [2]. Fishman and Richards [7] applied the Poiseuille's equation in their experiment. However, the Poiseuille's equation neglects that the pressure wave propagation in fluid creates an oscillation motion of the wall in a radial direction. Moens and Korteweg [1] developed a simple equation called as the Moens–Korteweg equation to predict the pressure wave velocity in long straight thin tube filled with an inviscid fluid. Because the effects of viscosity of fluid, inertial and shear and bending deformations of a tube are neglected, the Moens–Korteweg equation can only derive the wave speed $c_w = \sqrt{Eh/[2(R-h/2)\rho_f]}$. Bergal [8] modified the Moens–Korteweg equation for a thick-walled tube. It was found that the inclusion of wall thickness in the calculations increases the wave speed by about 10% over that given by conventional Moens–Korteweg expression. The Klip model considers the longitudinal wave propagation through the wall only and the effect of the tube flexural deformation is neglected. The wave speed is $c_w = \sqrt{E/[\rho_f(1-\nu^2)]}$ [9].

Womersley [10] considered a thin walled tube and the linearized Navier–Stokes equations that the nonlinear convective acceleration terms were neglected. Meanwhile, the radial vibration of tube wall was neglected. According to these assumptions, only the Young and Lamb modes were found. Moreover, the Young and Lamb modes represent the pressure wave modes propagating in the fluid and in the wall, respectively. Note that neglecting the radial vibration of tube does not match the real wave performance of artery. Tsangaris and Drikakis [11] used the shell theory and the Navier–Stokes equation to simulate the pressure wave traveling in anisotropic elastic tube. The model neglected the effects of the radial vibration and the moving boundary between the tube and the fluid. Demiray [6] considered the dynamic relation between the inner pressure and the radial oscillation of a tube. But the effect of flexural deformation of a tube and the viscosity of fluid were neglected. Then only the Young mode which represent pressure wave propagating in the fluid could be derived. Wang, et al. [12,13] considered an artery system as a transmission system of the blood pressure wave. When the wave frequency of the artery was consistent to the natural frequency of a tissue, the transmission efficiency was the best. This model is called as the resonant model. However, this model was derived too roughly to investigate the effects of the pre-pressure, the flow velocity and the flexural and axial vibrations. Lin et al. [2] investigated the wave modes of an elastic thin tube conveying blood. A new mathematical theory was proposed to describe the wave propagation through the elastic tube filled with viscous and incompressible fluid. The radial, axial and flexural vibrations of a tube wall are introduced simultaneously. In fact, the blood tube is tethered to surrounding tissue. The supporting effect of surrounding tissue on the wave propagation in the blood tube is not considered in the literature. The effect is not considered by Lin et al. [2]. Hodis and Zamir [14,15] investigated the effect of surrounding tissue on the shear stress in the tube wall. The cases of fully tethered and free walls and the complex Young's modulus were considered. But the radial displacement was neglected and all properties were independent to the longitudinal axis. So far, no literature studies the wave propagation in the thick-walled blood tube tethering to surrounding tissue.

In this paper, the mathematical theory for a thick-walled tube with the supporting effect of surrounding tissue on the wave propagation in the blood tube is investigated.

2. Governing equation of motion

2.1. Motion of an elastic tube

Consider an artery as uniform isotropic elastic thick tube [2]. The blood flows in the tube. In general, the critical threshold between laminar and turbulent flow is usually in the neighborhood of 2300. The mean average Reynold number in ascending aorta of an adult man is about 1500. Thus the flow field is laminar [16]. When any pulse wave generates from the heart, the energy is propagated via the blood and the tube. Meanwhile, there is the coupled motion of the tube and the blood. In order to investigate the coupled motion, the dynamic behavior of the tube is simulated by using the thick shell theory, as shown in Fig. 1. The blood flow field is simulated later. The assumptions about the tube are as follows:

a. The angle due to bending and the rotary inertia are considered.
b. The shear deformation in the x–r plane is considered.
c. The effect of tube bending is considered.
d. The plane cross section of a tube wall remains plane during deformation.
e. The axial symmetry is considered. The displacement $u_\theta = 0$ and the parameters are independent of the θ-axis.

It is well known that due to rough simplification one can obtain only one mode of the system such as the Young mode [1] and the Lame mode [9]. In the present model, three modes will be obtained simultaneously. These should be the lower and fundamental modes dominating in the real system. So far, the relevant mechanism is not clearly investigated. It is expected that if the nonlinear, anisotropic and non-axial symmetry effects are considered, the higher modes will be found. It is helpful

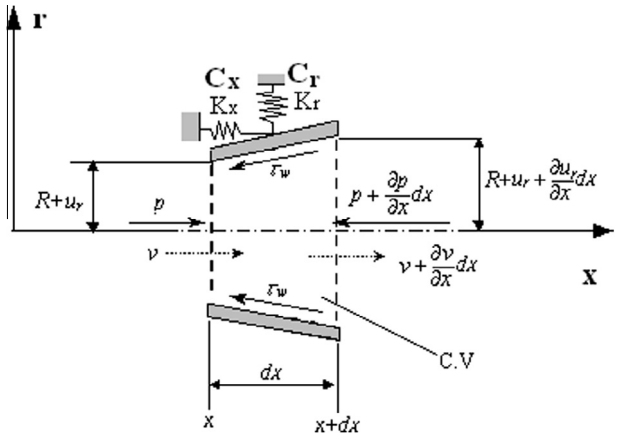

Fig. 1. Control volume of liquid flow in a circular cylinder.

to more accurately understanding the performance of wave propagation of artery. However, the system becomes too complicated to solve analytically so far. The relevant investigation will be made in future.

The equilibrium equations of motion in the thick-walled tube theory are [13]

$$\frac{1}{R}\left[c_{11}Rh\frac{\partial^2 u}{\partial x^2}+c_{11}\frac{h^3}{12}\frac{\partial^2\beta}{\partial x^2}+c_{12}h\frac{\partial w}{\partial x}\right]+\tau_w=I_0\frac{\partial^2 u}{\partial t^2}+I_1\frac{\partial^2\beta}{\partial t^2}+K_x u+C_x\frac{\partial u}{\partial t}, \tag{1}$$

$$Gh\left(\frac{\partial\beta}{\partial x}+\frac{\partial^2 w}{\partial x^2}\right)-\frac{1}{R}\left[c_{12}h\frac{\partial u}{\partial x}+c_{11}(\ln R_o-\ln R_i)w\right]+p=I_0\frac{\partial^2 w}{\partial t^2}+K_r w+C_r\frac{\partial w}{\partial t}, \tag{2}$$

$$\frac{c_{11}h^3}{12R}\frac{\partial^2 u}{\partial x^2}+\frac{c_{11}h^3}{12}\frac{\partial^2\beta}{\partial x^2}-Gh\left(\beta+\frac{\partial w}{\partial x}\right)=I_1\frac{\partial^2 u}{\partial t^2}+I_2\frac{\partial^2\beta}{\partial t^2}, \tag{3}$$

where the relevant derivation is presented in Appendix. The coefficients are

$$I_0=\rho_s h,\quad I_1=\frac{\rho_s h^3}{12R},\quad I_2=\frac{\rho_s h^3}{12}. \tag{4}$$

Considering the tube wall is tethered, the viscoelastic foundation constants K and C are given.

2.2. Coupled motion of fluid and tube

2.2.1. Conservations of momentum and mass

When a wave propagates through a tube, the flow field in the tube is assumed to be well developed. In addition, no slip condition at the wall should be considered. This condition is not considered by Lin et al. [2]. Therefore, the modified velocity distribution is expressed as

$$\eta=\frac{\partial}{\partial t}\left[u(x,t)-\frac{h}{2}\beta(x,t)\right]+\eta_{\max}(x,t)\left[1-\left(\frac{r}{R_i+w}\right)^2\right]. \tag{5}$$

The average shear stress at the wall is

$$\tau_w=\mu\frac{\partial}{\partial r}\left(\eta+\frac{1}{2}\frac{\partial\eta}{\partial z}dz\right)_{wall}. \tag{6a}$$

Considering $w << R$, one can obtain

$$\tau_w(x,t)\approx 2\mu\eta_{\max}/R_i. \tag{6b}$$

It is well known that the conservation of linear momentum for liquid is, as shown in Fig. 1.

$$F_b+F_s=\frac{\partial}{\partial t}\int_{c.v.}\vec{v}\rho_f d\nu+\int_{c.s.}\vec{v}\rho_f\vec{v}\cdot\hat{n}dA, \tag{7}$$

where the body force F_b is negligible here. The surface force is

$$F_s=-\left(p+\frac{\partial p}{\partial x}dx\right)\cdot\pi\left(R_i+w+\frac{\partial w}{\partial x}dx\right)^2+p\pi(R+w)^2-\tau_w\cdot 2\pi R_i\cdot dx. \tag{8}$$

Substituting the shear stress (6b) at the wall into Eq. (7) and considering a small amplitude, i.e., $w << R$, the momentum equation can be written as

$$\begin{aligned}&\left[-2pR_i\frac{\partial w}{\partial x}-\frac{\partial p}{\partial x}(R_i^2+2R_iw)-4\mu\eta_{\max}\right]\\&=\rho_f\left\{\left[\frac{\partial^2 u}{\partial t^2}-\frac{h}{2}\frac{\partial^2\beta}{\partial t^2}\right]R_i^2+2R_i\left[\frac{\partial u}{\partial t}-\frac{h}{2}\frac{\partial\beta}{\partial t}\right]\frac{\partial w}{\partial t}\right\}+\frac{1}{2}\rho_f R_i\left[R_i\frac{\partial\eta_{\max}}{\partial t}+2\left(\frac{\partial\eta_{\max}}{\partial t}w+\frac{\partial w}{\partial t}\eta_{\max}\right)\right]\\&+\rho_f\left[\begin{array}{l}\left(2\left(\frac{\partial u}{\partial t}-\frac{h}{2}\frac{\partial\beta}{\partial t}\right)\left(\frac{\partial^2 u}{\partial t\partial x}-\frac{h}{2}\frac{\partial^2\beta}{\partial t\partial x}\right)+\left(\frac{\partial^2 u}{\partial t\partial x}-\frac{h}{2}\frac{\partial^2\beta}{\partial t\partial x}\right)\eta_{\max}+\left(\frac{\partial u}{\partial t}-\frac{h}{2}\frac{\partial\beta}{\partial t}\right)\frac{\partial\eta_{\max}}{\partial x}+\frac{2}{3}\eta_{\max}\frac{\partial\eta_{\max}}{\partial x}\right)(R_i+w)^2\\+\left(\left(\frac{\partial u}{\partial t}-\frac{h}{2}\frac{\partial\beta}{\partial t}\right)^2+\left(\frac{\partial u}{\partial t}-\frac{h}{2}\frac{\partial\beta}{\partial t}\right)\eta_{\max}+\frac{1}{3}\eta_{\max}^2\right)2(R_i+w)\frac{\partial w}{\partial x}\end{array}\right].\end{aligned}\tag{9}$$

Meanwhile, if the amplitude of wave is small, the mass conservative equation can be expressed as

$$6R_i\frac{\partial w}{\partial t}+\left\{2R_i\left[6\left(\frac{\partial u}{\partial t}-\frac{h}{2}\frac{\partial\beta}{\partial t}\right)+\eta_{\max}\right]\frac{\partial w}{\partial x}+(R_i^2+2R_iw)\frac{\partial\left[6\left(\frac{\partial u}{\partial t}-\frac{h}{2}\frac{\partial\beta}{\partial t}\right)+\eta_{\max}\right]}{\partial x}\right\}=0.\tag{10}$$

A new mathematical model simulating the wave propagation through an elastic thick-walled tube conveying a liquid has been derived here. These coupled equations of wave propagation model are composed of Eqs. (1)–(3) and (9) and (10).

3. Solution method

3.1. Relation between pressure and flow velocity

Consider that there exists a pre-stressed pressure and a flow rate in the tube. When a wave propagates through a tube conveying a liquid, the pressure and the velocity can be assumed to be

$$p(x,t)=p_0(x)+p_1(z,t),\quad \eta_{\max}(x,t)=\eta_0(x)+\eta_1(x,t),\tag{11}$$

where $p_{0,z}$ is the pre-stressed steady pressure at the position of z, p_1 the disturbed wave pressure, $\eta_{\max_0}$ the average maximum flow velocity corresponding the given flow rate, and $\eta_{\max_1}$ the disturbed wave flow velocity.

In general, a steady pressure loss Δp through a tube is determined by using the Darcy–Weisbach equation as follows:

$$\Delta p=f\frac{L}{D}\frac{\rho_f\eta_a^2}{2},\tag{12}$$

where η_a is the average flow velocity which is determined via Eq. (5) and $\eta_a=\eta_{\max_0}/2$. L is the tube length, D is the diameter of the tube, and f is the friction factor. In this study, because the flow is laminar, the friction factor $f=64/\mathrm{Re}$. Substituting it back into Eq. (12), the pressure gradient is

$$\frac{dp_0}{dx}=\frac{-4\mu\eta_0}{R_i^2}.\tag{13}$$

3.2. Small propagation and linearization of general system

In general, because the elastic wave propagation is small, the disturbed wave pressure and velocity $\{p_1,\eta_{max1}\}$ are small. Substituting Eqs. (11) and (13) back into the coupled non-linear governing equations (1)–(3), (9) and (10) and considering the condition of small wave propagation, the coupled governing equations are linearized as follows:

$$\frac{1}{R}\left[c_{11}Rh\frac{\partial^2 u}{\partial x^2}+c_{11}\frac{h^3}{12}\frac{\partial^2\beta}{\partial x^2}+c_{12}h\frac{\partial w}{\partial x}\right]+\frac{2\mu\eta_{\max}}{R_i}=I_0\frac{\partial^2 u}{\partial t^2}+I_1\frac{\partial^2\beta}{\partial t^2}+K_xu+C_x\frac{\partial u}{\partial t},\tag{14}$$

$$Gh\left(\frac{\partial\beta}{\partial x}+\frac{\partial^2 w}{\partial x^2}\right)-\frac{1}{R}\left[c_{12}h\frac{\partial u}{\partial x}+c_{11}(\ln R_o-\ln R_i)w\right]+p=I_0\frac{\partial^2 w}{\partial t^2}+K_rw+C_r\frac{\partial w}{\partial t},\tag{15}$$

$$\frac{c_{11}h^3}{12R}\frac{\partial^2 u}{\partial x^2}+\frac{c_{11}h^3}{12}\frac{\partial^2\beta}{\partial x^2}-Gh\left(\beta+\frac{\partial w}{\partial x}\right)=I_1\frac{\partial^2 u}{\partial t^2}+I_2\frac{\partial^2\beta}{\partial t^2},\tag{16}$$

$$-\frac{\partial(p_0+p_1)}{\partial x}R_i^2-4\mu(\eta_0+\eta_1)=\rho_fR_i^2\left[\frac{\partial^2 u_1}{\partial t^2}-\frac{h}{2}\frac{\partial^2\beta_1}{\partial t^2}\right]+\frac{1}{2}\rho_fR_i^2\frac{\partial\eta_1}{\partial t},\tag{17}$$

$$6\frac{\partial w}{\partial t}+\left(2\eta_0\frac{\partial w}{\partial x}+R_i\left(\frac{d\eta_0}{dx}+\frac{\partial \eta_1}{\partial x}\right)+2\frac{d\eta_0}{dx}w\right)=0. \tag{18}$$

It is found that if the axial elastic foundation constant K_x is infinite, i.e., $\gamma_{x1}=1$, the axial displacement is zero i.e., $u=0$. If the radial elastic foundation constant K_r is infinite, i.e., $\gamma_{r1}=1$, the radial displacement is zero i.e., $w=0$. Moreover, if the elastic foundation constants K_x and K_r are infinite, the wall is **fully tethered**. If the elastic foundation constants K_x and K_r are zero, the wall is completely **free** from tethering. If the elastic foundation constants K_x and K_r are finite, the wall is **partially tethered**. Therefore, the degree of tethering can be clearly described by using the elastic foundation constants. Further, the effects of the elastic foundation constants on the wave speed and energy propagation are investigated later.

3.3. Characteristic equation

The wave solutions of Eqs. (14)–(18) can be expressed as

$$\eta_{\max}=\eta_0+\eta_1=\eta_0(x)+\bar{\eta}_1e^{i(kx-\omega t)},\quad p=p_0+p_1=p_0(x)+\bar{p}_1e^{i(kx-\omega t)},\quad u=u_0+u_1=u_0(x)+\bar{u}_1e^{i(kx-\omega t)},$$
$$w=w_0+w_1=w_0(x)+\bar{w}_1e^{i(kx-\omega t)},\quad \beta=\beta_0+\beta_1=\beta_0(x)+\bar{\beta}_1e^{i(kx-\omega t)}. \tag{19}$$

Substituting Eq. (19) into Eqs. (14)–(18), the general system is divided into two subsystems as following:

(a) Dynamic subsystem is composed of five following equations:

$$\bar{\eta}_1=\frac{4\omega}{kR_i}\bar{w}_1+2i\omega\left(\bar{u}_1-\frac{h}{2}\bar{\beta}_1\right), \tag{20}$$

$$\bar{p}_1=\frac{\rho_f}{(ik)}\left[\omega^2(\bar{u}_1-\frac{h}{2}\bar{\beta}_1)+\left(\frac{i\omega}{2}-\frac{4\mu}{\rho_fR_i^2}\right)\bar{\eta}_1\right], \tag{21}$$

$$a_1\bar{u}_1+a_2\bar{w}_1+a_3\bar{\beta}_1=0, \tag{22a}$$

where

$$\bar{a}_1=\gamma_{x2}\left(-c_{11}hk^2+I_0\omega^2+i\omega C_x+\frac{4\mu i\omega}{R_i}\right)-\gamma_{x1},$$

$$\bar{a}_2=\gamma_{x2}\left[\frac{ic_{12}hk}{R}+\frac{8\mu\omega}{R_i^2k}\right],$$

$$\bar{a}_3=\gamma_{x2}\left(-c_{11}\frac{h^3k^2}{12R}+I_1\omega^2-\frac{2\mu i\omega h}{R_i}\right),$$

$$\gamma_{x1}=\frac{K_x}{1+K_x},\quad \gamma_{x2}=\frac{1}{1+K_x}. \tag{22b}$$

$$b_1\bar{u}_1+b_2\bar{w}_1+b_3\bar{\beta}_1=0, \tag{23a}$$

where

$$\bar{b}_1=\gamma_{r2}\left[\frac{-ic_{12}hk}{R}-\frac{8\mu\omega}{kR_i^2}\right],$$

$$\bar{b}_2=\gamma_{r2}\left[-Ghk^2-\frac{c_{11}(\ln R_o-\ln R_i)}{R}+I_0\omega^2-K_r+i\omega C_r+\left(\frac{2\rho_f\omega^2}{k^2R_i}+\frac{16\mu i\omega}{k^2R_i^3}\right)\right]-\gamma_{r1},$$

$$\bar{b}_3=\gamma_{r2}\left[iGhk+\frac{4h\mu\omega}{kR_i^2}\right],$$

$$\gamma_{r1}=\frac{K_r}{1+K_r},\quad \gamma_{r2}=\frac{1}{1+K_r} \tag{23b}$$

$$c_1\bar{u}_1+c_2\bar{w}_1+c_3\bar{\beta}_1=0 \tag{24a}$$

where

$$c_1 = -\frac{c_{11}h^3k^2}{12R} + I_1\omega^2, \quad c_2 = -Gh(ik), \quad \text{and} \quad c_3 = -\frac{c_{11}h^3k^2}{12} - Gh + I_2\omega^2. \tag{24b}$$

(b) Static subsystem is composed of three following equations:

$$\frac{1}{R}\left[c_{11}Rh\frac{d^2u_0}{dx^2} + c_{11}\frac{h^3}{12}\frac{d^2\beta_0}{dx^2} + c_{12}h\frac{dw_0}{dx}\right] + \frac{2\mu\eta_0}{R_i} = K_x\left[u_0 + \frac{h}{2}\beta_0\right], \tag{25}$$

$$Gh\left(\frac{d\beta_0}{dx} + \frac{d^2w_0}{dx^2}\right) - \frac{1}{R}\left[c_{12}h\frac{du_0}{dx} + c_{11}(\ln R_o - \ln R_i)w_0\right] + p_0 - K_r w_0 = 0, \tag{26}$$

$$\frac{c_{11}h^3}{12R}\frac{d^2u_0}{dx^2} + \frac{c_{11}h^3}{12}\frac{d^2\beta_0}{dx^2} - Gh\left(\beta_0 + \frac{dw_0}{dx}\right) = 0, \tag{27}$$

$$-(R_i^2 + 2R_iw_0)\frac{dp_0}{\partial x} - 2R_ip_0\frac{dw_0}{dx} - 4\mu\eta_0 = \frac{1}{3}\rho_f\left[2R_i\eta_0^2\frac{dw_0}{dx} + 2R_i^2\eta_0\frac{d\eta_0}{\partial x} + 4R_i\eta_0\frac{d\eta_0}{\partial x}w_0\right], \tag{28}$$

$$2R_i\eta_0\frac{dw_0}{dx} + R_i^2\frac{d\eta_0}{dx} + 2R_i\frac{d\eta_0}{dx}w_0 = 0. \tag{29}$$

Note that Eqs. (25)–(29) are the relations among the static displacements, $\{u_0, w_0, \beta_0\}$, the pre-pressure p_0 and flow velocity η_0. Obviously, if the small deformation of tube is considered, Eq. (28) becomes to be the same as Eq. (13).

In the dynamic subsystem, Eqs. (22)-(24) can be expressed as

$$\begin{bmatrix} \bar{a}_1 & \bar{a}_2 & \bar{a}_3 \\ \bar{b}_1 & \bar{b}_2 & \bar{b}_3 \\ c_1 & c_2 & c_3 \end{bmatrix}\begin{bmatrix} \bar{u}_1 \\ \bar{w}_1 \\ \bar{\beta}_1 \end{bmatrix} = \begin{bmatrix} 0 \\ 0 \\ 0 \end{bmatrix}. \tag{30}$$

As a result, the dispersion equation of this dynamic system is obtained

$$\begin{vmatrix} \bar{a}_1 & \bar{a}_2 & \bar{a}_3 \\ \bar{b}_1 & \bar{b}_2 & \bar{b}_3 \\ c_1 & c_2 & c_3 \end{vmatrix} = 0. \tag{31}$$

4. Energy propagation

It is well known that the wave energy is stored in both the tube and the liquid. Milnor [1] found by experiment that for an *in situ* artery, over 90% of the energy is stored in the arterial wall and less than 10% is stored in the blood flow. However, the mechanism about the wave energy propagation has not been completely and clearly investigated yet. In this study, the energy transmission via different mode is investigated.

The energy propagation stored in the liquid is a product of the pressure p and the flow velocity η and expressed as following:

$$E_l = \int_A \langle p(t), \eta(t)\rangle dA, \tag{32}$$

where the average energy rate is $\langle p(t), \eta(t)\rangle = \int_0^T \mathrm{Re}(p)\mathrm{Re}(\eta)dt/T$. The energy in the tube is composed of the normal strain energy and the shear strain energy and is written as

$$E_t = \int_A \langle \sigma_x, \partial u_x/\partial t\rangle dA + \int_A \langle \tau_{rx}, \partial u_r/\partial t\rangle dA, \tag{33}$$

where the average normal strain energy is $\langle \sigma_x, \partial u_x/\partial t\rangle = \int_0^T \mathrm{Re}(\sigma_x)\mathrm{Re}[\partial u_x/\partial t]dt/T$ and the average shear strain energy is $\langle \tau_{rx}, \partial u_r/\partial t\rangle = \int_0^T \mathrm{Re}(\tau_{rx})\mathrm{Re}[\partial u_r/\partial t]dt/T$. Substituting the pressure and the flow velocity of a wave mode into Eq. (32) and the stresses and the displacements of a wave mode into Eq. (33), the corresponding energy propagations stored in the blood liquid and the tube can be obtained.

5. Numerical results

Given a wave frequency ω, one can easily find four sets of conjugated complex wave numbers of Eq. (31), $k_n(\omega) = k_{r,n}(\omega) \pm ik_{i,n}(\omega), n = 1, 2, 3, 4$. Each set of conjugated roots represent both a forward wave and a backward wave,

respectively. If $k_{i,n}$ is positive, the wave amplitude decays with a forward wave. But if $k_{i,n}$ is negative, the wave amplitude increases with a forward wave. This solution is trivial. Based on these facts, one can obtain the dispersion curves of several wave modes. In this study, the wave propagation through both the blood and the artery are considered. One finds that three sets of conjugated roots are reasonable, but one is trivial. Each reasonable solution represents one wave mode. In summary, the wave energy is propagated in terms of three kinds of wave modes shown in Fig. 2.

Fig. 2 shows the influence of the wave frequency on the three mode shapes. Firstly, it is observed that the first mode is dominated by a radial displacement of a tube wall. The deformation of tube does not depend on the wave frequency. However, the influence of the wave frequency on the fluid velocity is significant. When the wave frequency is small, the fluid velocity is very small. It implies that when the wave frequency is small, the majority of the wave energy must be propagated through the tube in the bending motion. However, increasing the wave frequency significantly increases the fluid velocity. It means that when the wave frequency is large, the majority of the wave energy is propagated through both the tube in the bending motion and the fluid.

Secondly, the second mode is usually called as the Young mode. It is an axial motion of a tube accompanying small radial and bending motions of a tube and relatively very large amplitude of fluid velocity. Therefore, the majority of the wave energy must be propagated through fluid in the pressure wave motion. Finally, the third mode is usually called as the Lamb mode. It is a large axial motion of a tube accompanying the negligible radial and bending motions of a tube. The influence of the wave frequency on the fluid velocity is significant. When the wave frequency is small, the ratio of the fluid velocity and the axial motion is very small. Therefore, the majority of the wave energy must be propagated through the tube in the axial motion. It is consistent to the traditional phenomenon of the Lamb mode. When the wave frequency is large enough, the ratio of the fluid velocity and the axial motion becomes significant. In other words, the majority of the wave energy is propagated through both the tube in the axial motion and the fluid. The physical and material properties in Fig. 2 are considered later.

Moreover, several methods are used to investigate the dispersion curves of the Young mode. Fig. 3a shows that the numerical results by using the present thick-walled tube theory and the thin-walled tube theory [2] are compared with those by Womersley [10], Wang et al. [12], Cox [17] and Mirsky [18]. It is found that the wave speed determined by Wang et al. [12] is overestimated and that by Cox [17] is underestimated. In this case the ratio of the tube thickness to the tube radius h/R is 0.13. The numerical results by using the present thick-walled tube theory and the thin-walled tube theory [2] are almost consistent. Further, Fig. 3b shows the relation between the transmission per wavelength and the wave frequency of the second or Young mode without the elastic foundation. It is observed that the transmission per wavelength increases with the wave frequency. If the wave frequency is large enough, the transmission per wavelength approaches constant. Moreover, it is found that the transmission determined by Wang et al. [12] is over estimated. The numerical results by using the present thick-walled tube theory and the thin-walled tube theory [2] are almost consistent.

Fig. 4 show the comparison of the thin-walled tube theory [2] and the present thick-walled tube theory with different ratio h/R. It is found that the effect of the ratio h/R on the relation between the wave speed and the wave frequency is great. Moreover, the larger the ratio h/R is, the more the difference between the wave speed in the present thick-walled tube theory

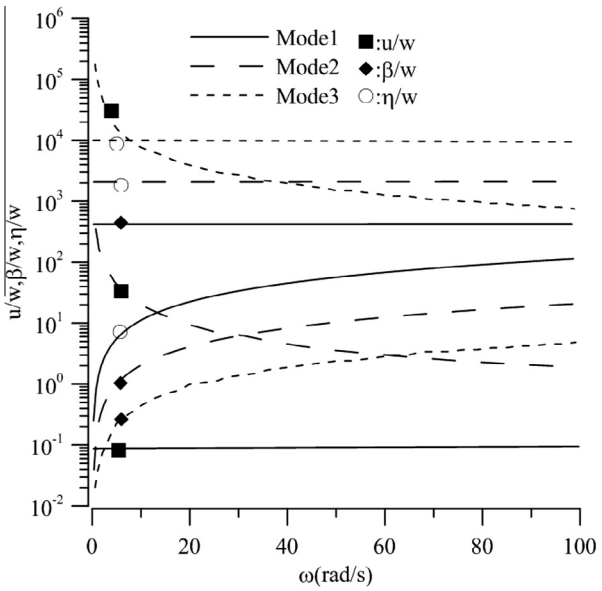

Fig. 2. Influence of wave frequency ω on the three kinds of mode shapes. [$\gamma_{r1} = \gamma_{x1} = 0$, $v = 0.5$, $E = 1.6$ MPa, $R_o = 0.13$ cm, $h = 0.039$ cm, $\rho_s = 1100$ kg/m^3, $\rho_f = 1056$ kg/m^3, $\mu = 3.5 \times 10^{-3}$ N · s/m^2, $p_0 = 7466$ Pa].

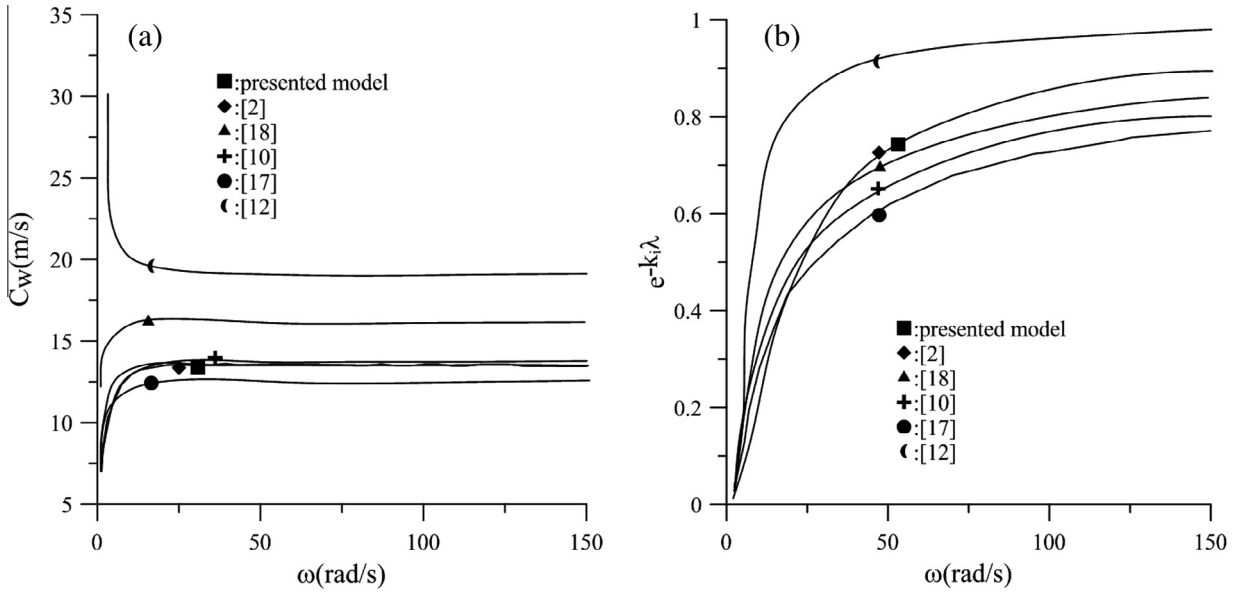

Fig. 3. Comparison of wave speeds and dispersion curves of the second mode in different models. [$\gamma_{r1} = \gamma_{x1} = 0$, $\nu = 0.5$, $E = 3$ MPa, $R_o = 0.23$ cm, $h = 0.03$ cm, $\rho_t = 1100$ kg/m^3, $\rho_f = 1056$ kg/m^3, $\mu = 3.5 \times 10^{-3}$ N · s/m^2, $p_0 = 10$ kPa].

and that in the thin-walled tube theory for the first and second modes but not for the third mode. The reason can be found from the mode shapes shown in Fig. 2 that the first and second modes include both the flexural and shear deformations. But for the third mode the axial motion dominates.

Based on the relations (32) and (33), one can determine the quantities of energy transmission through the tube and the liquid or blood. As shown in Fig. 5, the effect of the ratio h/R on the relation between the energy transmission through the tube and the wave frequency is significant. Increasing the ratio h/R increases the energy transmission through the tube for the second mode. It is because the flexural motion dominates for the second mode. In other hand, increasing the ratio h/R decreases the energy transmission through the tube for the third mode. It is because the axial motion dominates for the third mode. Moreover, the larger the ratio h/R is, the more the difference between the energy transmission through the tube in the present thick-walled tube theory and that in the thin-walled tube theory for all the modes. It is also observed that about

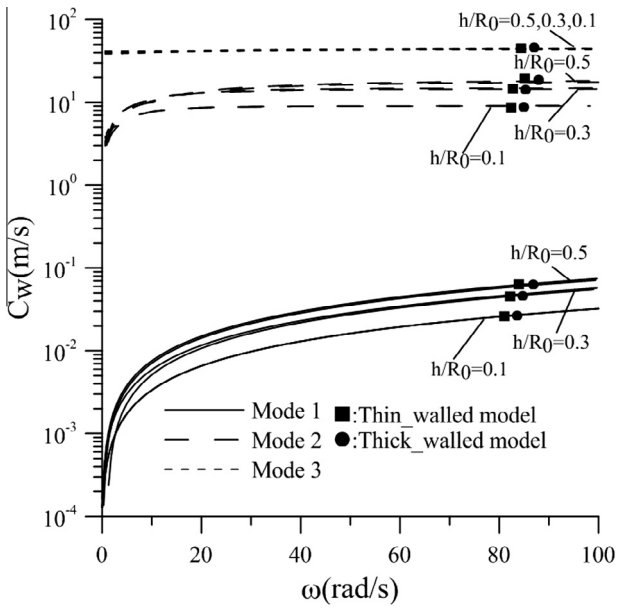

Fig. 4. Relation among the ratios h/R_0, the wave frequency ω and the wave speed c_w. [$\gamma_{r1} = \gamma_{x1} = 0$, $\nu = 0.5$, $E = 1.6$ MPa, $R_o = 0.13$ cm, $\rho_s = 1100$ kg/m^3, $\rho_f = 1056$ kg/m^3, $\mu = 3.5 \times 10^{-3}$ N · s/m^2, $p_0 = 7466$ Pa].

99.8% and 95% of the energies of the first and third modes are transmitted through the tube. As to the second mode, if the wave frequency is large enough, only about 50% of the energy is transmitted through the tube. The detailed reasons are expressed as follows:

It has been found in Fig. 2 that the first mode is a wall flexural motion accompanying with a large fluid velocity. Because both the bending rigidity and the flexural deformation of a tube wall are large, almost all the wave energy is transmitted through the tube. The third mode is with a axial motion of a tube accompanying with a negligible radial motion and a large flow velocity. Therefore, majority of the wave energy is also transmitted through the tube. However, the second mode is a large axial motion of a tube accompanying with small radial motion and very large flow velocity. It is well known that the flexural and axial motions of tube are neglected in the conventional Moens–Korteweg model for determining the Young

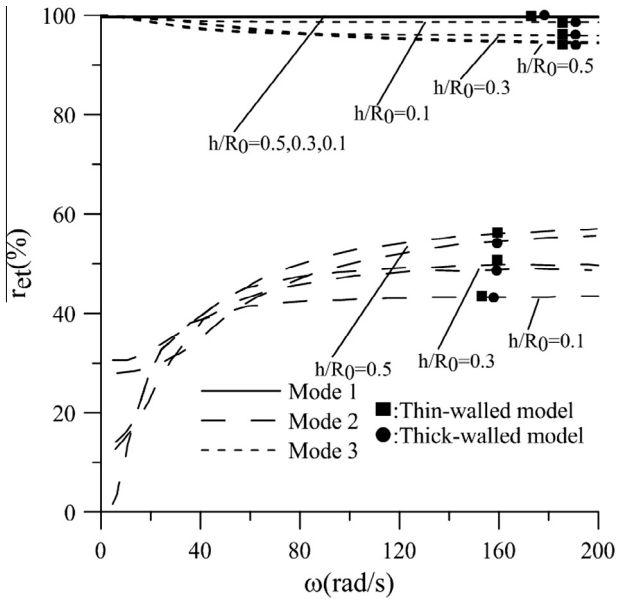

Fig. 5. Relation among the ratio h/R_0, the percentage of the energy transmission through the tube r_{et} and the wave frequency ω. [$v = 0.5$, $E = 1.6$ MPa, $R_o = 0.13$ cm, $\rho_s = 1100$ kg/m^3, $\rho_f = 1056$ kg/m^3, $\mu = 3.5 \times 10^{-3}$ N · s/m^2, $p_0 = 7466$ Pa, $\gamma_{r1} = \gamma_{x1} = 0$].

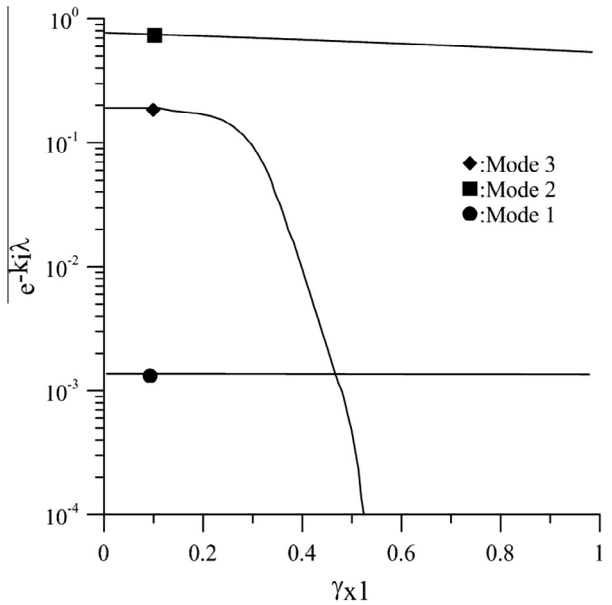

Fig. 6. Influence of the axial elastic foundation constant γ_{x1} on the transmission per wave length $e^{-k_i\lambda}$ for different modes [$\gamma_{r1} = 0$, $v = 0.5$, $E = 3$ MPa, $R_o = 0.23$ cm, $h = 0.03$ cm, $\rho_z = 1100$ kg/m^3, $\rho_f = 1056$ kg/m^3, $\mu = 3.5 \times 10^{-3}$ N · s/m^2, $p_0 = 10$ kPa].

mode. According to this simplification, it is usually concluded that the Young mode represents the pressure wave propagation in the fluid and all the energy is transmitted through the liquid. It is not reasonable. In this study, Fig. 5 shows that about 50% of the wave energy is transmitted through the tube.

Further, the effects of the elastic foundations on the mode shapes, the wave speed and the energy propagation are investigated here.

Fig. 6 shows that if there is no the axial elastic foundation, i.e., $\gamma_{x1} = 0$, the transmissions per wave length of the first and second mode are smallest and largest, respectively. The effect of the axial elastic foundation constant γ_{x1} on the transmissions of the first mode is negligible. However, if $\gamma_{x1} \geqslant 0.51$, increasing the constant γ_{x1} decreases significantly the transmission for the third mode. Moreover, the third transmission approaches to zero. In other word, the third mode disappears due to the increasing of the elastic foundation constant γ_{x1}. Further, Fig. 7 demonstrates that if there is no the axial elastic foundation, i.e., $\gamma_{x1} = 0$, the energy transmission through the tube for the first, second and third modes are about 100%, 24% and

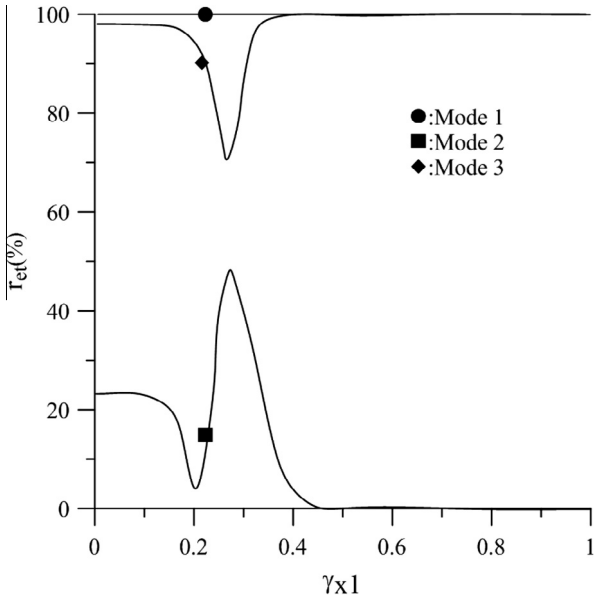

Fig. 7. Influence of the axial elastic foundation constant γ_{x1} on the percentage of energy propagations through the tube r_{et} for different modes with the same parameters as those given in Fig. 5.

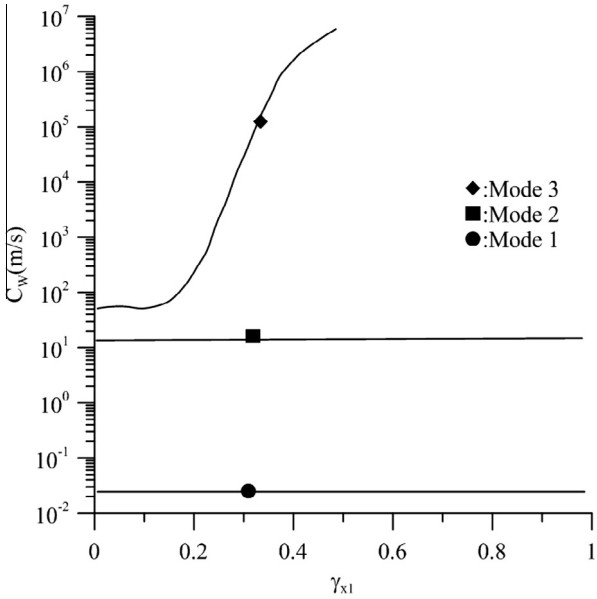

Fig. 8. Influence of the axial elastic foundation constant γ_{x1} on wave speeds c_w for different modes with the same parameters as those given in Fig. 5.

96%, respectively. The effect of the elastic foundation constant on the energy transmission ratio of the first mode is negligible. However, if $0.15 < \gamma_{x1} < 0.4$, the effect of the elastic foundation constant on the energy transmission ratio of the second and third modes is significant. Moreover, Fig. 8 shows that increasing the constant γ_{x1} increases obviously the wave speed for the third mode. It is because the axial rigidity is increased.

Fig. 9 shows that if the radial elastic foundation constant $\gamma_{r1} < 0.5$, the effect of the constant on the transmission per wave length of the three modes is negligible. When $0.5 < \gamma_{r1} < 0.63$, the effect of the constant γ_{r1} on the three transmissions becomes significant. Increasing the constant γ_{r1}, the first transmission is abruptly decreased. if $\gamma_{r1} \geqslant 0.63$, the first transmission approaches to zero. In other word, the first mode disappears. It is because for the first mode the radial displacement dominates. The radial displacement decreases with the radial foundation constant γ_{r1}. When $0.5 < \gamma_{r1} < 0.63$, the

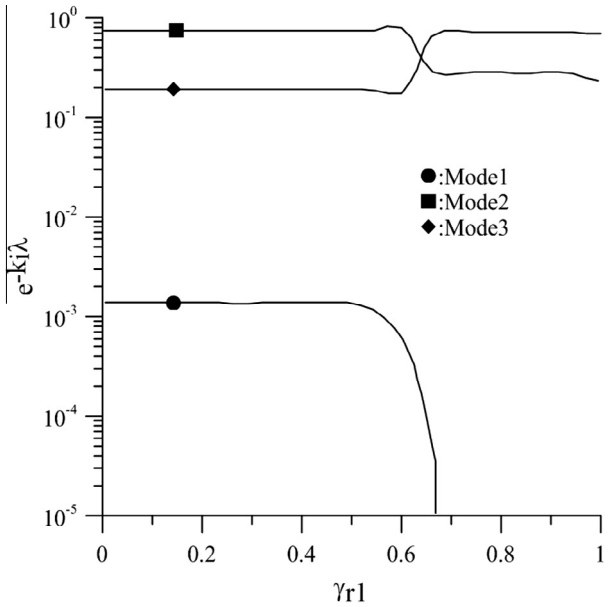

Fig. 9. Influence of the radial elastic foundation constant γ_{r1} on the transmission per wave length $e^{-k_i\lambda}$ for different modes [$\gamma_{x1} = 0$, $\nu = 0.5$, $E = 3$ MPa, $R_o = 0.23$ cm, $h = 0.03$ cm, $\rho_s = 1100$ kg/m^3, $\rho_f = 1056$ kg/m^3, $\mu = 3.5 \times 10^{-3}$ N · s/m^2, $p_0 = 10$ kPa].

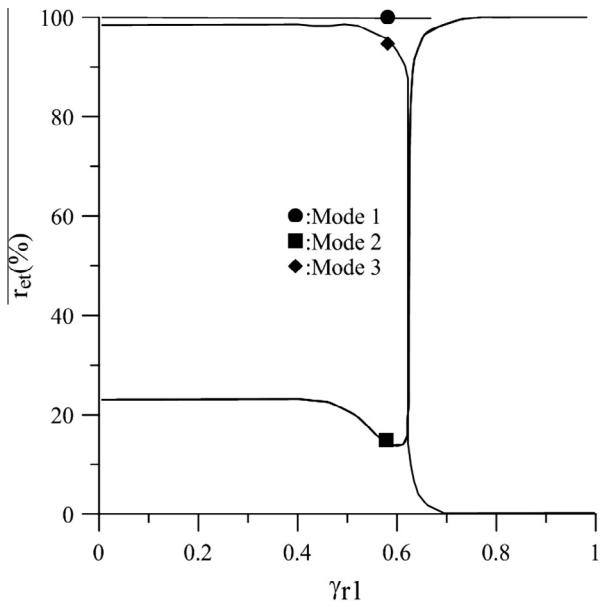

Fig. 10. Influence of the radial elastic foundation constant γ_{r1} on the percentage of energy propagations through the tube r_{et} for different modes with the same parameters as those given in Fig. 8.

transmission of the second modes decreases significantly with the constant γ_{r1}. Further, when $\gamma_{r1} \geqslant 0.63$, the transmission for the second mode is almost constant. The reverse phenomenon happens for the third mode. Further, Fig. 10 demonstrates that if there is no the radial elastic foundation, i.e., $\gamma_{r1} = 0$, the energy transmission through the tube for the first, second and third modes are about 100%, 24% and 96%, respectively. If $0.5 < \gamma_{r1} < 0.63$, the effect of the elastic foundation constant on the energy transmission ratio of the second and third modes is significant. The energy transmission ratio through the tube for the third mode will greatly decrease to zero at $\gamma_{r1} = 0.63$. However, if $\gamma_{r1} > 0.63$ the energy transmission ratio of the second mode becomes from about 24% to 100%. Moreover, Fig. 11 shows that the constant γ_{r1} is increased over the critical value of 0.63, the wave speed for the third mode is increased significantly. It is because the radial rigidity is increased.

It is found in Fig. 6 that if the axial elastic foundation is infinite, i.e., $\gamma_{x1} = 1$, the axial displacement u is zero and the third mode disappears. There is no radial elastic foundation i.e., $\gamma_{r1} = 0$ in Figs. 6–8. Further, one investigates the effect of the

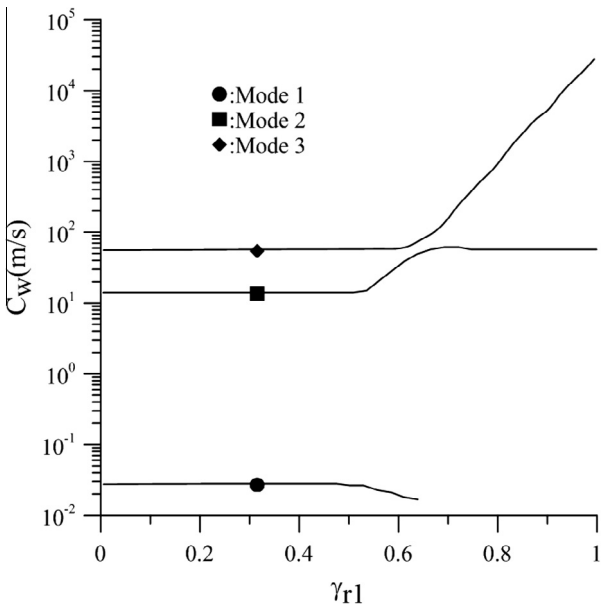

Fig. 11. Influence of the radial elastic foundation constant γ_{r1} on wave speeds c_w for different modes with the same parameters as those given in Fig. 8.

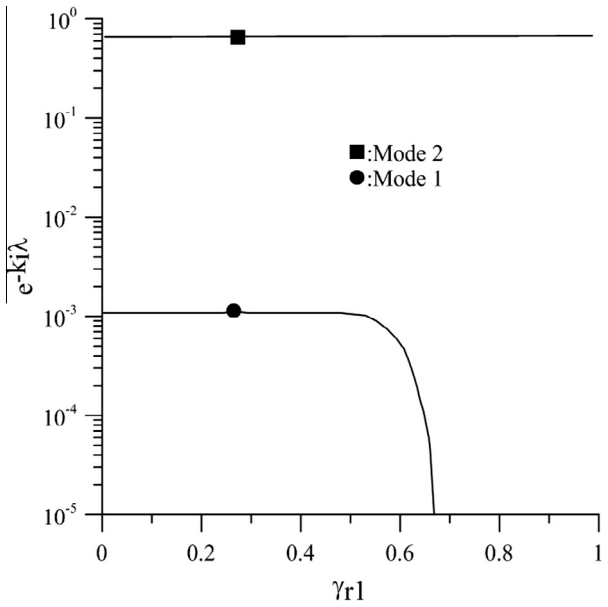

Fig. 12. Influence of the radial elastic foundation constant γ_{r1} on the transmission per wave length $e^{-k_i\lambda}$ for different modes [$\gamma_{x1} = 1$, $\nu = 0.5$, $E = 3$ MPa, $R_o = 0.23$ cm, $h = 0.03$ cm, $\rho_s = 1100$ kg/m^3, $\rho_f = 1056$ kg/m^3, $\mu = 3.5 \times 10^{-3}$ N · s/m^2, $p_0 = 10$ kPa].

radial elastic foundation constant on the wave propagation under $\gamma_{x1} = 1$. Fig. 12 shows that the effect of the constant on the transmission per wave length of the second mode is negligible. It is different to that in Fig. 9 without the axial elastic foundation, i.e., $\gamma_{x1} = 0$. Moreover, if the radial elastic foundation constant $\gamma_{r1} < 0.5$, the effect of the constant on the transmission per wave length of the two modes is negligible. But when $0.5 < \gamma_{r1} < 0.63$, increasing the constant γ_{r1} the first transmission is abruptly decreased and approaches to zero at $\gamma_{r1} \geqslant 0.63$. In other word, the first mode disappears. Further, Fig. 13 demonstrates that if $\gamma_{x1} = 1$, the effect of the radial elastic foundation constant γ_{r1} on the energy transmission ratio of the first two modes is negligible. Moreover, Fig. 14 shows that the constant γ_{r1} is increased over the critical value of 0.6, the wave speed for the second mode is increased significantly. It is because the radial rigidity is increased.

Fig. 15 demonstrates the effect of the longitudinal and radial damping constants $\{C_x, C_r\}$ on the waves speed. It is found that the larger the longitudinal damping constant C_x is, the lower the waves speed of mode 3 is. However, its effect on those of modes 1 and 2 is negligible. It is because the longitudinal displacement of tube dominates in mode 3. Moreover, the effect

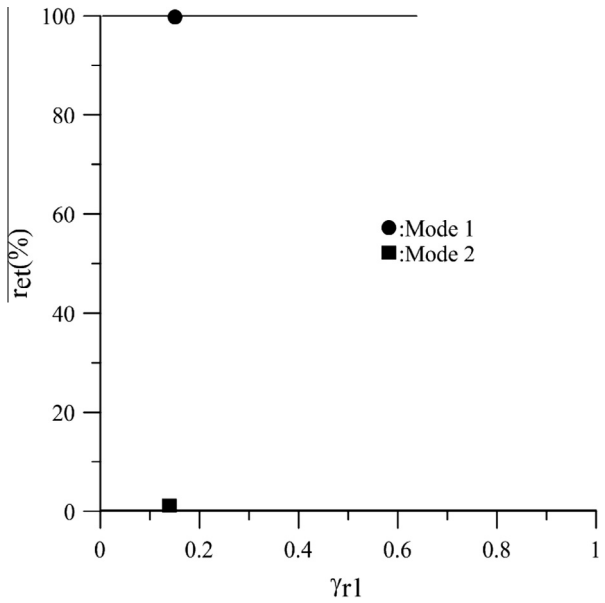

Fig. 13. Influence of the radial elastic foundation constant γ_{r1} on the percentage of energy propagations through the tube r_{et} for different modes with the same parameters as those given in Fig. 11.

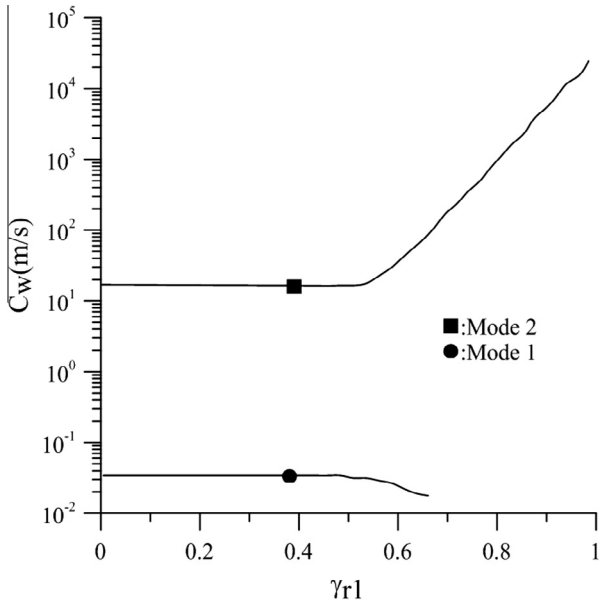

Fig. 14. Influence of the radial elastic foundation constant γ_{r1} on the wave speeds c_w for different modes with the same parameters as those given in Fig. 11.

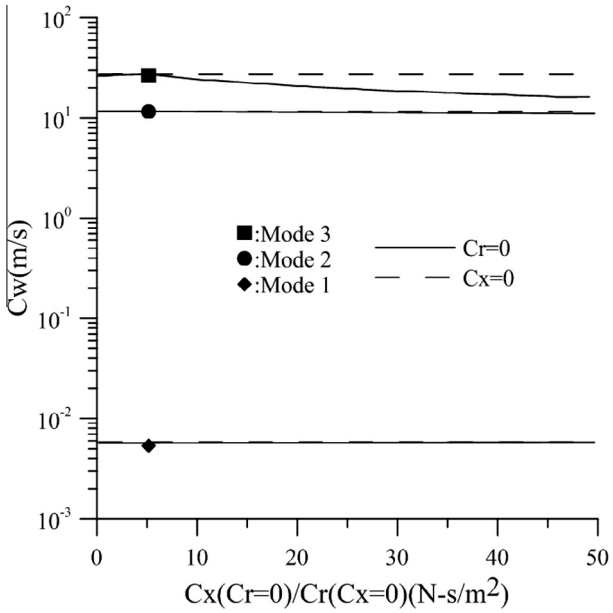

Fig. 15. Influence of the longitudinal and radial damping constants $\{C_x, C_r\}$ on the wave speeds c_w for different modes with the same parameters as those given in Fig. 11.

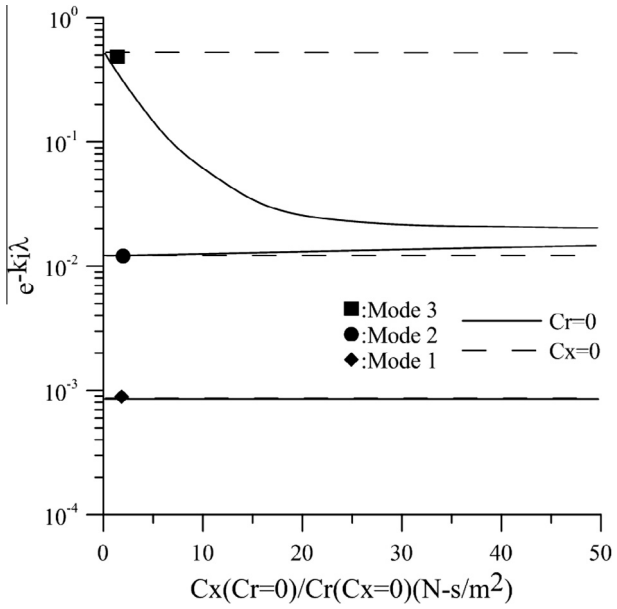

Fig. 16. Influence of the longitudinal and radial damping constants $\{C_x, C_r\}$ on the transmission per wave length $e^{-k_i\lambda}$ for different modes with the same parameters as those given in Fig. 11.

of the radial damping constant C_r on the wave speeds of the three modes is negligible. Further, Fig. 16 demonstrates the effect of the longitudinal and radial damping constants $\{C_x, C_r\}$ on transmission. It is found that the larger the longitudinal damping constant C_x is, the lower the transmission of mode 3 is. However, its effect on those of modes 1 and 2 is negligible. Moreover, the effect of the radial damping constant C_r on the transmissions of the three modes is negligible.

6. Conclusion

This paper presents a new model for simulation of wave propagation in an elastic thick tube conveying blood. The analytical solution for the system is derived. By using this new theory, the flexural, Young and Lamb modes can be obtained

simultaneously. If the wave frequency is large enough, about {99.8%, 50%, 95%} of the energies of the first, second and third modes are transmitted through the tube. Moreover, the transmissions per wavelength of the three modes are about {0.1%, 20%, 85%}, respectively. Based the fact of transmission, the first wave mode will firstly disappear in short time. Secondly the second mode will disappear. Finally the third mode dominates. About 95% of the energy of the third mode through the artery tube is easily discovered. This conclusion is consistent to the experiment given by Milnor [1]. The larger the ratio h/R is, the more the difference between the wave speed in the present thick-walled tube theory and that in the thin-walled tube theory for the first and second modes but not for the third mode. Moreover, the effect of the viscoelastic foundation constants $\{\gamma_{x1}, \gamma_{r1}, C_x\}$ on the wave speed, the energy transmission through the tube r_{et} and the transmission per wavelength $e^{-k_i\lambda}$ is significant. The main phenomena are revealed:

(1) When $0.5 < \gamma_{r1} < 0.63$, increasing the constant γ_{r1} the first transmission per unit wave length is abruptly decreased greatly. When the constant γ_{r1} is increased to the critical value of 0.63, the flexural motion of artery tube (1st mode) disappears.
(2) When $0.3 < \gamma_{x1} < 0.51$, increasing the constant γ_{x1} the third transmission per unit wave length is abruptly decreased greatly. When the constant γ_{x1} is increased to the critical value of 0.51, the longitudinal motion of artery tube (3rd mode) disappears.
(3) If the elastic foundation constants are infinite, i.e., $\gamma_{r1} = \gamma_{x1} = 1$, the tube wall is fully tethered. Moreover, the first and third modes disappear.
(4) The lower the waves speed and transmission of mode 3 are, the larger the longitudinal damping constant C_x.

Because the flexural and longitudinal motions of artery tube are actually allowed, the dimensionless foundation constants $\{\gamma_{r1}, \gamma_{x1}\}$ should be less than $\{0.5, 0.3\}$, respectively. However, it is helpful for understanding the overall effect of foundation on the wave propagation of the piping system supported by any foundation.

Acknowledgment

The support of the National Science Council of Taiwan, ROC, is gratefully acknowledged (Grant number: Nsc99-2212-E168-016).

Appendix A. Relations among forces, moments, strain and curvatures of the thick-walled model

The displacement fields are as following:

$$u_x = u(x,t) + (r-R)\beta(x,t), \quad u_\theta = 0, \quad u_r = w(x,t). \tag{A1}$$

It should be noted that the angle due to bending β is an independent variable. However, for the thin-walled model $\beta = \partial w/\partial x$. Moreover, the rotary inertia and the shear deformation are not considered. The corresponding strains are [19]

$$\varepsilon_x = \frac{\partial u}{\partial x} + (r-R)\frac{\partial \beta}{\partial x}, \quad \varepsilon_r = 0, \quad \varepsilon_\theta = \frac{w}{r}, \quad \gamma_{x\theta} = 0, \quad \gamma_{r\theta} = 0, \quad \gamma_{xr} = \frac{\partial w}{\partial x}. \tag{A2}$$

The first subscript indicates the face. The second one indicates the direction. The corresponding stresses can be determined via the Hook's law as following:

$$\begin{bmatrix} \sigma_x \\ \sigma_\theta \\ \sigma_r \\ \tau_{x\theta} \\ \tau_{r\theta} \\ \tau_{xr} \end{bmatrix} = \begin{bmatrix} c_{11} & c_{12} & c_{12} & 0 & 0 & 0 \\ c_{12} & c_{11} & c_{12} & 0 & 0 & 0 \\ c_{12} & c_{12} & c_{11} & 0 & 0 & 0 \\ 0 & 0 & 0 & (c_{11}-c_{12})/2 & 0 & 0 \\ 0 & 0 & 0 & 0 & (c_{11}-c_{12})/2 & 0 \\ 0 & 0 & 0 & 0 & 0 & (c_{11}-c_{12})/2 \end{bmatrix} \begin{bmatrix} \varepsilon_x \\ \varepsilon_\theta \\ \varepsilon_r \\ \gamma_{x\theta} \\ \gamma_{r\theta} \\ \gamma_{xr} \end{bmatrix}, \tag{A3}$$

where $c_{11} = \frac{E(1-\nu)}{(1-2\nu)(1+\nu)}$, $c_{12} = \frac{E\nu}{(1-2\nu)(1+\nu)}$ and $(c_{11}-c_{12})/2 = \frac{E}{2(1+\nu)} = G$. Moreover, the relations among the forces, the moments, the strain and the curvatures are [16]

$$\begin{aligned} (N_x, Q_x, N_{x\theta}) &= \int_{R_i}^{R_o} (\sigma_x, \tau_{xr}, \tau_{\theta x}) \frac{r}{R} dr, \quad (N_\theta, N_{\theta x}, Q_\theta) = \int_{R_i}^{R_o} (\sigma_\theta, \tau_{\theta x}, \tau_{\theta r}) dr, \quad (M_x, M_{xr}, M_{x\theta}) \\ &= \int_{R_i}^{R_o} (\sigma_x, \tau_{xr}, \tau_{x\theta}) \frac{r}{R}(r-R) dr, \quad M_\theta = \int_{R_i}^{R_o} \sigma_\theta z dz. \end{aligned} \tag{A4}$$

References

[1] W.R. Milnor, Hemodynamics, second ed., William & Wilkins, 1989.
[2] S.M. Lin, S.Y. Lee, C.C. Tsai, C.W. Chen, W.R. Wang, J.F. Lee, Wave modes of an elastic tube conveying blood, CMES Comput. Model. Eng. Sci. 34 (1) (2008) 33–54.
[3] D.J. Korteweg, Uber die Fortpflanzungsges-chwindigkeit des Schalles in elastischen Rohren. Ann. Phys. Chem. (NS) 5, 525.
[4] W. Harvey, Movement of the Heart and Blood in Animals, William Fitzer, Frankurt, 1628.
[5] S. Hales, Statical Essays: Containing Haemastaticks, 1733.
[6] H. Demiray, Wave in initially stressed fluid-filled thick tubes, J. Biomech. 30 (3) (1997) 273–276.
[7] A.P. Fishman, D.W. Richards, Circulation of the Blood. Men and Ideas, Oxford University Press, New York, 1964.
[8] D.H. Bergel, The dynamic elastic properties of the arterial wall, J. Physiol. 156 (1961) 458–469.
[9] W. Klip, P. Van Loon, D.A. Klip, Formulas for phase velocity and damping of axial waves in thick-walled viscous tubes, J. Appl. Phys. 38 (1968) 3745–3755.
[10] J.R. Womersley, Oscillatory motion of a viscous liquid in a thin-walled elastic tube. I. The linear approximation for long waves, Philos. Mag. 46 (1955) 199–221.
[11] S. Tsangaris, D. Drikakis, Pulsating blood flow in an initially stressed, anisotropic elastic tube: linear approximation of pressure waves, Med. Biol. Eng. Comput. 27 (1) (1989) 82–88.
[12] Y.Y.L. Wang, C.C. Chang, J.C. Chen, H. Hsiu, W.K. Wang, Pressure wave propagation in a distensible tube arterial model with radial dilation, IEEE Eng. Med. Biol. Mag. 16 (1997) 51–56.
[13] Y.Y.L. Wang, W.C. Lia, H. Hsiu, M.Y. Jan, W.K. Wang, Effect of length on the fundamental resonance frequency of arterial models having radial dilatation, IEEE Trans. Biomed. Eng. 47 (3) (2000) 313–318.
[14] S. Hodis, M. Zamir, Mechanical events within the arterial wall: the dynamic context for elastin fatigue, J. Biomech. 42 (2009) 1010–1016.
[15] S. Hodis, M. Zamir, Mechanical events within the arterial wall under the forces of pulsatile flow: a review, J. Mech. Behavior Biomed. Mater. 4 (8) (2011) 1595–1602.
[16] David N. Ku, Blood flow in arteries, Annu. Rev. Fluid Mech. 9 (1997) 399–434.
[17] R.H. Cox, Wave propagation through a Newtonian fluid contained within a thick-walled viscoelastic tube: the influence of wall compressibility, Biophys. J. 3 (1970) 317–355.
[18] I. Mirsky, Wave propagation in a viscous fluid contained in an orthotropic elastic tube, Biophys. J. 7 (1968) 165–186.
[19] I. Mirsky, Vibrations of orthotropic, thick, cylindrical shells, J. Acoust. Soc. Am. 36 (1) (1964) 41–51.